High Sensitive Z-shaped Fiber Interferometric Refractive Index Sensor: Simulation and Experiment

Journal:	*Photonics Technology Letters*
Manuscript ID	PTL-34235-2018
Manuscript Type:	Original Paper
Date Submitted by the Author:	29-Jan-2018
Complete List of Authors:	Ma, Youqiao; Dalhousie University, Department of Electrical and Computer Engineering GUO, DI; Nova Scotia Community College, School of trades and technology Sarah, Sabrina; Dalhousie University, Department of electrical and computer Engineering Gao, Yangyuanlong; Dalhousie University, Department of electrical and computer Engineering Wu, Qiang; Northumbria University, Physics and Electrical Engineering; Dublin Institute of Technology, Photonics Research Centre, School of Electrical and Electronics Engineering Zhou, Jun; Institute of Photonics, Faculty of Science Pistora, Jaromir; Technical University Ostrava, Physics Cada, Michael; Dalhousie University, Department of Electrical and Computer Engineering;
Key Words:	Optical fiber devices, Interferometry, Sensitivity

High Sensitive Z-shaped Fiber Interferometric Refractive Index Sensor: Simulation and Experiment

Youqiao Ma*, Di Guo, Sabrina Sarah, Yangyuanlong Gao, Qiang Wu, Jun Zhou, Jaromír Pištora, Michael Cada

***Abstract*—A robust fiber-optic interferometer, which is formed by introducing two bends (i.e. z shape) to the standard telecommunication single mode fiber, is designed and analyzed theoretically and experimentally for the refractive index (RI) sensing. The first (second) bend couples (re-couples) the core (cladding) mode to the cladding (core) modes. The RI-sensitive phase difference between the core and cladding modes gives rise to the modulation of the transmitted intensity. The experimental results show that the z-shaped interferometric sensor possesses an RI sensitivity as high as 196 nm/RIU, which is much higher than that of the similar existing interferometric sensor and fit well with the theoretical predictions. An investigation of the effect of perturbations of bent angle reveals that the sensor possesses relative high sensitivities as the bent angle ranges from 13° to 17° with difference between the maximum and minimum sensitivities only 2.5% indicating the structure has a good fabrication tolerance to the inaccuracy of the bent angles. In addition, the sensor has advantages of low cost, simple structure and ease of fabrication, showing great potential in many sensing applications.**

***Index Terms*—Fiber sensors, Interferometer**

I. INTRODUCTION

Because of the advantages including small size, high sensitivity and immunity to electromagnetic interference, optical fiber sensors have been extensively investigated over the last decade for various physical and chemical sensing applications, such as temperature, vibration, stress and refractive index (RI) [1-6]. Particularly, the RI measurement is an important process in many fields, e.g., the detection of solution concentration in chemical field [7], real-time monitoring of antigen-antibody recognition in biological field [8] and water quality control in environmental field [9].

This work was supported by Natural Sciences and Engineering Research Council of Canada (NSERC); Collaborative Research and Training Experience (CREATE); Applied Science in Photonics and Innovative Research in Engineering of Canada (ASPIRE); Grand Agency of Czech Republic (#15-21547S); and National Natural Science Foundation of China (NSFC) (61320106014 and 61675104).

Youqiao Ma, Sabrina Sarah, Yangyuanlong Gao and Michael Cada are with Department of electrical and computer Engineering, Dalhousie University, Halifax, Canada (e-mail: mayouqiao188@hotmail.com).

Di Guo is with School of trades and technology, Nova Scotia Community College, Halifax, Canada

Qiang Wu is with Department of physics and electrical engineering, Northumbria University, Newcastle, United Kingdom

Jun Zhou is with Institute of Photonics, Faculty of Science, Ningbo University, Ningbo, China

Jaromír Pištora is with Nanotechnology Centre, VSB Technical University of Ostrava, Ostrava-Poruba, Czech Republic.

The implementation of optical fiber sensors is usually based on two mechanisms, which are the evanescent field coupling (EFC) [10] and mode interference (MI) [11], respectively. In recent years, numerous EFC-based fiber configurations were proposed, for example by utilizing the long period fiber grating (LPFG) [12], the tilted fiber Bragg grating (TFBG) [13] and the surface plasmon resonance (SPR) [14]. LPFG and TFBG operate in the evanescent field of cladding mode, which exists closing to the fiber surface and easily spreads into the surrounding target solution, thus suffer from a large insertion loss [15]. SPR technique utilizes the highly-localized evanescent wave propagating along the interface between a dielectric and metal, which is very sensitive to the variations of the surrounding RI in the vicinity of metal surface [16]. However, the inherent metallic loss results in the broaden linewidth and low measurement accuracy [17]. On the other hand, the interferometric fiber sensors are becoming one of the most attractive approaches for RI sensing because of their flexible configurations and high sensitivities [18]. Reported interferometric fiber sensors include designs based on core-offset fibers [19], z-shaped fibers [20], singlemode-multiomode-singlemode (SMS) fibers [21], photonic crystal fibers [22], micro-tapered fibers [23] and Fabrt-Perot (FP) cavities [24]. Compared to the other fiber interferometers, the z-shaped configuration has additional advantages of low cost and ease of fabrication. The operating principle of z-shaped fiber sensors is based on the mode interference between the fundamental core mode and cladding modes which are excited by the fiber bend [25]. Thus, the z-shaped fibers can be used to measure the temperature and strain [20]. Previous design shows that a z-shaped fiber can also act as a RI sensor which possesses a linear sensitivity of 185 nm/refractive index unit (RIU) in the RI range of 1.333-1.381 [25]. So far, however, the systemic studies of z-shaped fiber structures are rarely reported and it is worthwhile taking further investigations for the first time with aim of optimizing the key physical parameters of a z-shaped fiber used as an interferometer. Therefore, in this paper we theoretically and experimentally carry out a detailed analysis of RI sensing performance for a z-shaped fiber interferometer, taking into account the influence of the bent angles. Experimental verification is carried out demonstrating an average RI sensitivity of 196 nm/RIU.

II. DEVICE MODEL AND PRINCIPLE

Figure 1 (a) schematically shows the configuration of the z-shaped fiber interferometer. The middle portion of the z segment has a length of L, and it is bent by two angles of α and β, respectively. All the structural characteristics and coordinate system are depicted in Fig. 1 (a). The fiber used in the simulations and experiments is the standard communication single mode fiber (SMF-28), which has a core diameter of 8.3 μm and the refractive indices of the core and cladding are 1.4504 and 1.4447, respectively. Fig. 1 (b) depicts the contour plot of simulated light energy distribution along the z-shaped fiber at a wavelength of 1550 nm utilizing a wide-angle beam propagation method (WABPM) in cylindrical coordinates with the

perfect matched layer (PML) boundary conditions, and Fig. 1 (c) shows the normalized power of fundamental core mode along the propagation direction. In this simulation, the structural parameters are selected as L = 5 mm, $\alpha = \beta = 10^{o}$, and the values of the curvature radius and arc angle around the corners are set as 4.5 mm and 15°, respectively. As can be seen from Fig. 1 (b), the fundamental core mode spreads into the fiber cladding when it arrives at the first bend in the z segment, or in other words, the cladding modes are excited due to the asymmetric refractive index profile, giving rise to the reduced power of core mode as shown in Fig. 1 (c). Therefore, the first bend of the z segment functions as a beam splitter. On contrary, the core and cladding modes will recombine together at the second bend which acts as a beam combiner, resulting in an increased power of core mode as seen in Fig. 1 (c). Thus, an interferometer is formed.

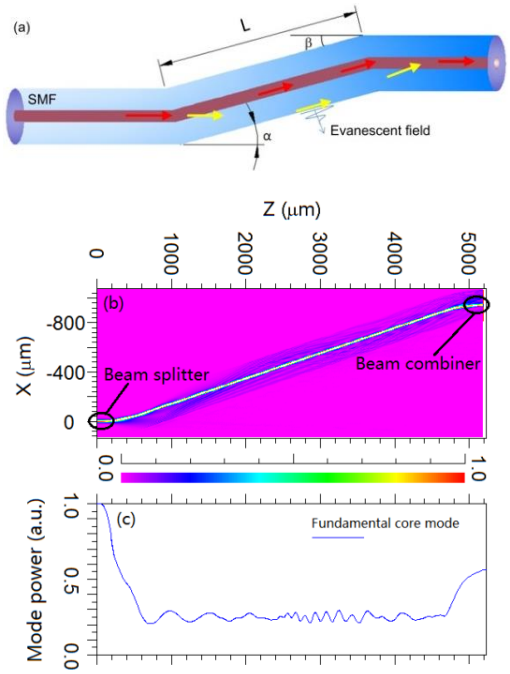

Fig.1 (Color online) (a) Schematic diagram of z-shaped fiber interferometer. (b) Energy distribution along z-shaped fiber interferometer at wavelength of 1550 nm. (c) Normalized power of fundamental core mode along propagation.

After travelling by a distance of L, the phase difference between the core and cladding modes can be described as:

(1)

where $\Delta\beta_m = 2\pi(n_{eff}^{co} - n_{eff}^{cl,m})/\lambda$ is the wave-vector difference between the core mode and m-th cladding mode, in which λ is the wavelength of incident light, n_{eff}^{co} and $n_{eff}^{cl,m}$ are the effective refractive indices of the core mode and m-th cladding mode, respectively. When the light arrives at the second bend of z segment, the core mode interferes with the cladding modes, resulting in a modulation of the transmitted intensity I_t, which is given by:

$$+ \sum_m I_{cl}^m + 2\sum_m \sqrt{I_{co} I_{cl}^m} \cos(\Delta\phi_m) \quad (2)$$

where I_{co} and I_{cl}^m are the light intensities of the core mode and m-th cladding mode, respectively.

According to Eq. (4), a change in the RI of the surrounding environment will cause a change in the effective refractive indices of cladding modes thus causes the variations of the interference and the transmitted intensity, revealing the basis of the sensing scheme.

III. RESULTS AND DISCUSSIONS

To analyze the practical sensing performance of the z-shaped fiber interferometer, the experiments were carried out. Fig. 2 (a) illustrates the measurement setup. Light from an amplified spontaneous emission (ASE) source was launched into the z-shaped fiber which is located on a glass substrate and the transmission spectrum was recorded by an optical spectrum analyzer (OSA). The inset in Fig. 2 (a) shows an example of a microscope image of the z-shape fiber with parameters of α (β) = 15° and L = 8 mm, which was fabricated by employing the electric arc method. Fig. 2 (b) depicts a local picture of the fusion splicing window. The fabrication process involves: (1) One side of the fiber is fixed by a built-in holder clamp, while another side is fixed on a three-dimensional (3D) translation stage. (2) By precisely moving the 3D stage towards the splicer, the fiber between the discharge electrodes slightly curves as shown in Fig. 2 (b). (3) The first bend of z-shape is formed after the arc discharge. The discharge current and time were set as 12 mA and 6 s, respectively. (4) Repeating the steps (1-3) would form the second bend of z-shape and complete the structure. The distance between the two bends (i.e. the length of L) can be easily controlled by moving the 3D stage.

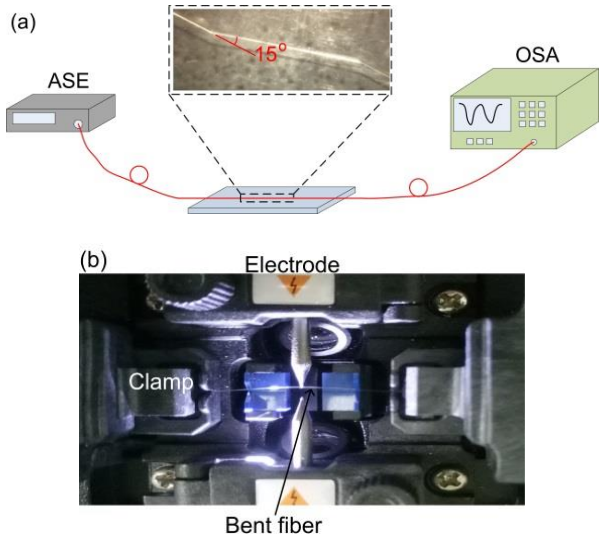

Fig.2 (Color online) (a) Diagram of measurement setup. Inset: microscope image of fabricated z-shaped fiber interferometer. (b) Schematic picture of fusion splicing window with bend fiber between two electrodes.

Figure 3 presents the calculated and measured transmission spectra of the z-shaped fiber structure in the water environment (n_{water} = 1.33) with different length L and bent angle $\alpha = \beta = 15^{o}$. As shown in Fig. 3, the obvious interference patterns are displayed. The suppression of transmission is due to the destructive interference between the core and cladding modes, and vice versa. With the increase of L, the interference pattern exhibits a faster oscillation, which is physically reasonable due to the fact that the interference period is inversely proportional to the length L, leading to a decreased valley linewidth. However, in order to minimize the physical size of the interferometer, a length of z segment of 8 mm is chosen for following numerical and experimental investigations. Moreover, through the further observation in Fig. 3, one can find that the measured results show a good agreement with theoretical prediction. The discrepancy between the calculated and measured results could

be due to the deformed shape of the fabricated z segment which could give rise to additional scattering loss.

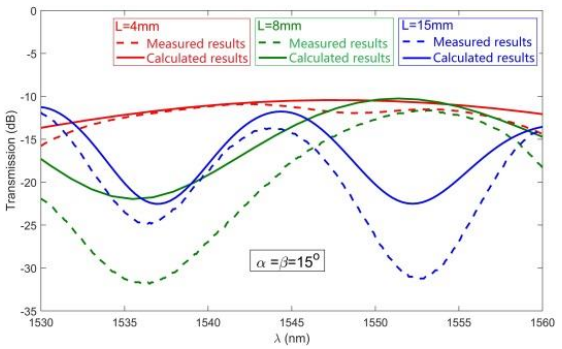

Fig.3 (Color online) Measured and calculated spectral responses of z-shaped fiber interferometer with different length *L* over a wavelength range of 1530-1560 nm.

The RI sensing measurements were performed at the room temperature (~ 23 °C) with a series of RI liquids, which were placed around the z segment (with bent angle $\alpha = \beta = 15^{o}$) by utilizing a dropper. The RIs of these liquids were controlled by adjusting the concentrations of glycerol solutions and collimated by an Abbe refractometer at 589 nm which possesses an RI error of ± 0.0002. After each test for each RI solution, the z segment sensor and glass slide were cleaned with ethanol and deionized water and dried by the compressed air. Fig. 4 (a) depicts the measured transmission spectra. It is found that as RI increases, the interference dip shifts toward a longer wavelength, which shows that the RI variations for the sample surrounding the z segment can be monitored by measuring the shift of the central dip wavelength. The simulated and experimental results of the wavelength vs. RI are plotted in Fig. 4 (b). The experimental results match the theoretical simulations reasonably well. As expected from measurements, the curve shows an essentially linear distribution with an average sensitivity of 196 nm/ RIU over an RI range of 1.33-1.38, which has been greatly enhanced compared with other simple types of fiber interferometers, such as recently reported core-offset [26] and dual-taper cascaded [27] fiber structures with sensitivities of 78.7 nm/ RIU and 62.78 nm/ RIU, respectively.

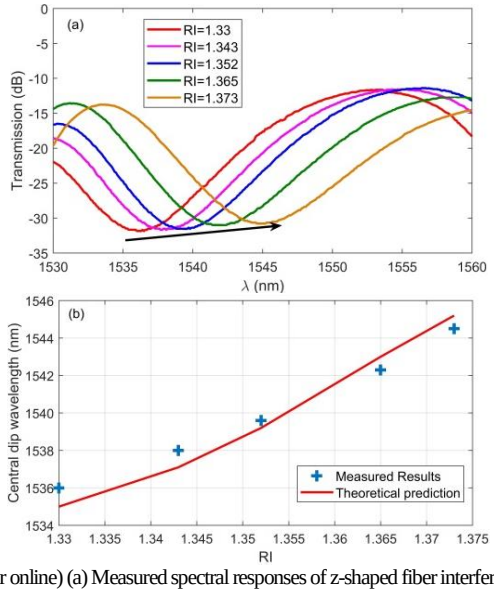

Fig.4 (Color online) (a) Measured spectral responses of z-shaped fiber interferometer over a wavelength range of 1530-1560 nm with different RI. (b) Measured and calculated central dip wavelength vs. different RI.

The influence of the bent angle (i.e. α and β) on the sensing performance was also investigated. Fig. 5 (a) shows the dependence of the sensitivity on the bent angle α while the bent angle β is fixed as $\beta = 15^{o}$. From it one can see that with the increase of the bent angle α, the sensitivity is shown to increase at first and then decreases, exhibiting high sensitivities as the bent angle ranges from 13^{o} to 17^{o}. To examine the physical mechanisms behind this phenomenon better, the normalized electromagnetic energy distributions for structures with the small bent angle α ($\alpha = 5^{o}$) and large angle α ($\alpha = 20^{o}$) are plotted in Fig. 5 (b) and 5 (c), respectively. From Fig. 5 (b) it is clear that the energy of the fundamental core mode almost keeps constant for the small bent angel α, or in other words, a small amount of cladding modes is excited. While when the bend angle α is large, as shown in Fig. 5 (c), the leakage of cladding modes takes place. In both cases, the interference between the core and cladding modes becomes weak, which could possibly give rise to the decreased sensitivity. Moreover, the inset in Fig, 5 (a) depicts the sensitivity as a function of bent angle β with $\alpha = 15^{o}$. From it one can note that the sensitivity is insignificantly dependent on the angle β. This is because of the fact that the interference between core and cladding modes is mainly determined by the first bent angle α. However it should note that the small or large angle β will affect the coupling from cladding modes back to core mode, which will reduce the transmitted intensity and decrease the interference pattern ratio. From the above discussion, one can see that, in order to realize the high sensitivity, the optimized angle range for α and β is from 13^{o} to 17^{o}. The difference between the maximum and minimum sensitivities within this range is only 2.5%, indicating that the z-shaped fiber interferometer possesses a good fabrication tolerance to the inaccuracy of the bent angles.

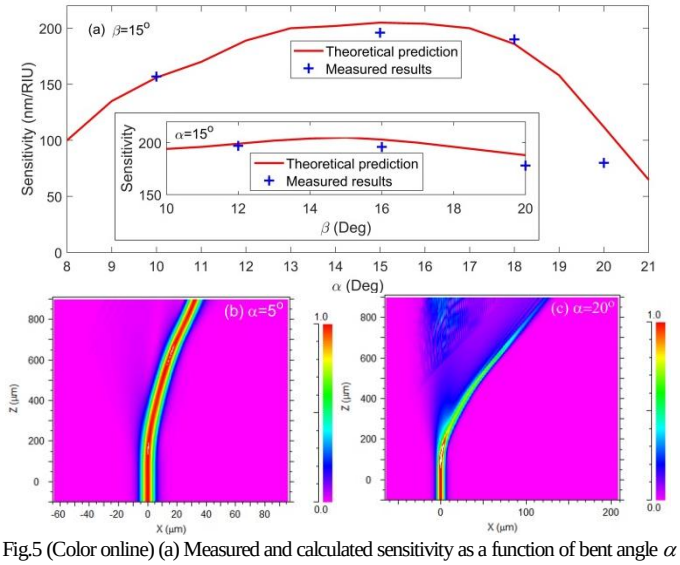

Fig.5 (Color online) (a) Measured and calculated sensitivity as a function of bent angle α with $\beta = 15^{o}$. Inset: Measured and calculated sensitivity as a function of bent angle β with $\alpha = 15^{o}$. Simulated light energy distributions around first bend with (b) $\alpha = 5^{o}$ and (c) $\alpha = 20^{o}$.

Finally, it is worth mentioning that in addition to the two bends in the studied z-shaped fiber interferometer, the interferometric concept can be extended by designing different so-called first splitting and second combining schemes, such as utilizing LPFG, TFBG, micro-taper, and so on, which are capable of converting core and cladding mode to each other [12, 13, 23]. We will apply these structures and compare their RI sensing performance in our future work.

IV. CONCLUSIONS

In conclusion, a novel and robust high sensitive z-shaped fiber-based interferometric refractive index sensor is theoretically and experimentally designed and demonstrated. The first bend of z segment couples core mode to high-order cladding modes. The phase difference between core and cladding modes is influenced by the surrounding refractive index environment. As a result, the field amplitudes of core and cladding modes interfere with each other, resulting in a modulation in the transmitted intensity at the second bend of z segment. With the optimized parameters, the experimental results show that the RI sensitivity could reach up 196 nm/ RIU, which is much higher compared to other recently reported types of interferometric sensors. Furthermore, in consideration of its attractive merits i.e., low cost, simple configuration and ease of fabrication, we believe it shows a great promise in many physical and chemical sensing fields.

REFERENCES

1. Z. Y. Li, C. R. Liao, D. N. Chen, J. Song, W. Jin, G. D. Peng, F. Zhu, Y. Wang, J. He, and Y. P. Wang, "Label-free detection of bovine serum albumin based on an in-fiber Mach-Zehnder interferometric biosensor," Opt. Express 25, 17105-17113 (2017).
2. S. L. Zhang, Z. W. Zhao, N. Chen, F. F. Pang, Z. Y. Chen, Y. Q. Liu, and T. Y. Wang, "Temperature characteristics of silicon core optical fiber Fabry-Perot interferometer," Opt. Lett. 40, 1362-1365 (2015).
3. T. Guo, F. Liu, B. O. Guan, and J. Albert, "Tilted fiber grating mechanical and biochemical sensors," Opt. Laser Technol. 78, 19-33 (2016).
4. W. J. Yu, T. T. Lang, J. C. Bian, and W. Kong, "Label-free fiber optic biosensor based on thin-core modal interferometer," Sens. Actuator B-Chem. 228, 322-329 (2016).
5. X. D. Wang, and O. S. Wolfbeis, "Fiber-optic chemical sensors and biosensors (2013-2015)," Anal. Chem. 88, 203-227 (2016).
6. Q. Wu, M. W. Yang, J. H. Yuan, H. P. Chan, Y. Q. Ma, Y. Semenova, P. F. Wang, C. X. Yu, and G. Farrell, "The use of a bend singlemode-multimode-singlemode (SMS) fibre structure for vibration sensing," Opt. Laser Technol. 63, 29-33 (2014).
7. H. Q. Yu, L. B. Xiong, Z. H. Chen, Q. G. Li, X. N. Yi, Y. Ding, F. Wang, H. Lv, and Y. M. Ding, "Solution concentration and refractive index sensing based on polymer microfiber knot resonator," Appl. Phys. Express 7, 022501 (2014).
8. Y. X. Huang, J. He, C. Y. Tan, and M. Luo, "Easy and rapid multi-pass detection of antigen and antibody with micro-lens sensors," Biosens. Bioelectron. 86, 1003-1010 (2016).
9. P. Matthew, W. Rebecca, W. J. Stephen, D. Frank, P. J. H. Seamus, and P. T. Ralph, "Long period grating based toluene sensor for use with water contamination," Sens. Actuator B-Chem. 203, 621-625 (2014).
10. A. Messica, A. Greenstein, and A. Katzir, "Theory of fiber-optic, evanescent-wave spectroscopy and sensors," Appl. Opt. 35, 2274-2284 (1996).
11. L. C. Li, L. Xia, Z. H. Xie, and D. M. Liu, "All-fiber Mach-Zehnder interferometers for sensing applications," Opt. Express 20, 11109-11120 (2012).
12. L. Melo, G. Burton, P. Kubik, and P. Wild, "Long period gratings coated with hafnium oxide by plasma-enhanced atomic layer deposition for refractive index measurements," Opt. Express 24, 7654-7669 (2016).
13. T. Guo, F. Liu, B. O. Guan, and J. Albert, "Tilted fiber grating mechanical and biochemical sensors," Opt. Laser Technol. 78, 19-33 (2016).
14. H. Agrawal, A. M. Shrivastav, B. D. Gupta, "Surface plasmon resonance based optical fiber sensor for atrazine detection using molecular imprinting technique," Sens. Actuator B-Chem. 227, 204-211 (2016).
15. A. Leung, P. M. Shankar, and R. Mutharasan, "A review of fiber-optic biosensors," Sens. Actuator B-Chem. 125, 688-703 (2007).
16. W. L. Barnes, A. Dereux, and T. W. Ebbesen, "Surface plasmon subwavelength optics," Nature 424, 824-830 (2003).
17. M. C. Estevez, M. A. Otte, B. Sepulveda, L. M. Lechuga, "Trends and challenges of refractometric nanoplasmonic biosensors: A review," Anal. Chim. Acta 806, 55-73 (2014).
18. M. R. Islam, M. M. Ali, M. H. Lai, K. S. Lim, and H. Ahmad, "Chronology of Fabry-Perot interferometer fiber-optic sensors and their applications: A review," Sensors 14, 7451-7488 (2014).
19. J. T. Zhou, Y. P. Wang, C. R. Liao, B. Sun, J. He, G. L. Yin, S. Liu, Z. Y. Li, G. J. Wang, X. Y. Zhong, and J. Zhao, "Intensity modulated refractive index sensor based on optical fiber Michelson interferometer," Sens. Actuator B-Chem. 208, 315-319 (2015).
20. C. Zhang, P. Lu, H. Liao, W. J. Ni, X. Fu, X. Y. Jiang, D. M. Liu, and J. S. Zhang, "Simultaneous measurement of axial strain and temperature based on a z-shaped fiber structure," IEEE Photon. J. 9, 6803608 (2017).
21. Q. Wu, Y. Semenova, P. F. Wang, and G. Farrell, "High sensitivity SMS fiber structure based refractometer – analysis and exeperiment," Opt. Express 19, 7937-7944 (2011).
22. C. Lin, Y. Wang, Y. J. Huang, C. R. Liao, Z. Y. Bai, M. X. Hou, Z. Y. Li, and Y. P. Wang, "Liquid modified photonic crystal fiber for simultaneous temperature and strain measurement," Photon. Res. 5, 129-133 (2017).
23. T. K. Yadav, R. Narayanaswamy, M. H. A. Bakar, Y. M. Kamil, and M. A. Mahdi, "Single mode tapered fiber-optic interferometer based refractive index sensor and its application to protein sensing," Opt. Express 22, 22802-22807 (2014).
24. Y. F. Wu, Y. D. Zhang, J. Wu, and P. Yuan, "Temperature-insensitive fiber optic Fabry-Perot interferometer based on special air cavity for transverse load and strain measurements," Opt. Express 25, 9443-9448 (2017).
25. R. Yang, Y. S. Yu, Y. Xue, C. Chen, Q. D. Chen, and H. B. Sun, "Single S-tapered fiber Mach-Zehnder interferometers," Opt. Lett. 36, 4482-4484 (2011).
26. Y. Zhao, X. G. Li, and L. Cai, "A highly sensitive Mach-Zehnder interferometeric refractive index sensor based on core-offset single mode fiber," Sens. Actuators A: Phys. 223, 119-124 (2015).
27. Q. Wang, C. Y. Li, C. W. Zhao, and W. Z. Li, "Guided-mode-leaky-guided-mode fiber interferometer and its high sensitivity refractive index sensing technology," Sensors 16, 801 (2016).